

## A SURVEY OF COMPACT STAR CLUSTERS IN THE S-W FIELD OF THE M 31 DISK. STRUCTURAL PARAMETERS. II

I. Šablevičiūtė<sup>1</sup>, V. Vansevičius<sup>1</sup>, K. Kodaira<sup>2</sup>, D. Narbutis<sup>1</sup>, R. Stonkutė<sup>1</sup> and A. Bridžius<sup>1</sup>

<sup>1</sup> Institute of Physics, Savanorių 231, Vilnius LT-02300, Lithuania,  
*wladas@astro.lt*

<sup>2</sup> The Graduate University for Advanced Studies (SOKENDAI),  
Shonan Village, Hayama, Kanagawa 240-0193, Japan

Received 2007 August 8; revised 2007 October 28; accepted 2007 October 30

**Abstract.** The King and the EFF (Elson, Fall & Freeman 1987) analytical models are employed to determine the structural parameters of star clusters using an 1-D surface brightness profile fitting method. The structural parameters are derived and a catalogue is provided for 51 star cluster candidates from the survey of compact star clusters in the South-West field of the M 31 disk performed by Kodaira et al. (2004).

**Key words:** galaxies: individual (M 31) – galaxies: spiral – galaxies: star clusters – globular clusters: general – open clusters: general

### 1. INTRODUCTION

Kodaira et al. (2004; hereafter Paper I) performed a survey of compact star clusters in the South-West field of the M 31 galaxy disk. The high-resolution Suprime-Cam imaging (Miyazaki et al. 2002) at the Subaru Telescope (National Astronomical Observatory of Japan) enabled us to resolve a large fraction of star clusters in M 31. Since the cluster sample consists of unresolved, semi-resolved and resolved objects, one needs to apply an appropriate method for consistent determination of their structural parameters.

In a previous study (Šablevičiūtė et al. 2006; hereafter Paper II) we derived cluster structural parameters by employing the widely used program package BAO-LAB/ISHAPE (Larsen 1999). However, the ISHAPE algorithm is designed to work best for objects whose intrinsic size, i.e., the Full Width at Half Maximum (FWHM) of the object luminosity distribution, is comparable to or is smaller than the FWHM of the star image Point Spread Function (PSF) (Larsen 2006). Therefore, it is difficult to apply ISHAPE for the analysis of semi-resolved clusters, in which a few resolved stars make the fitting parameter  $\chi^2$  more sensitive to the distribution of these stars than to the general shape of the cluster. On the other hand, for such objects a simple direct fit of the 1-D surface brightness profiles (see, e.g., Hill & Zaritsky 2006) is also not appropriate due to strong alteration of the cluster parameters by the PSF effects. Therefore, we use a method developed to derive the intrinsic structural parameters of clusters from 1-D surface brightness

profiles, altered by the PSF effects, using simulated star clusters convolved with PSF.

## 2. STAR CLUSTER SAMPLE

The M31 star cluster sample studied in this paper is described in detail in Papers I and II. Here we briefly remind only the most important features of the observations. We have used the Suprime-Cam  $V$ -band frames ( $5 \times 2$  min exposures) of the  $\sim 17.5' \times 28.5'$  size centered at  $0^{\text{h}}40.9', +40^{\circ}45'$  (J2000.0). For the study of the cluster structural parameters we have used the  $V$ -band stacked mosaic image of  $2 \times 3$  CCDs containing a total of  $\sim 6\text{K} \times 8\text{K}$  pixels (pixel size  $0.2'' \times 0.2''$ ). The typical FWHM of stellar images is  $\sim 0.7''$ . The morphological atlases and photometry results for prominent compact objects ( $17.5 \leq V \leq 19.5$ ) were presented in Paper I for 52  $\text{H}\alpha$  emission objects (KWE) and 49 non-emission clusters (KWC).

The cluster sample selected for the present study is listed in Table 1 of Paper II.  $UBVRI$  broad-band aperture CCD photometry data for these clusters were published by Narbutis et al. (2006). In this study we adopt the M31 distance modulus of  $m - M = 24.5$  (e.g., Stanek & Garnavich 1998).

## 3. STRUCTURAL PARAMETERS OF THE CLUSTERS

### 3.1. The surface brightness profiles

The surface brightness profiles of the clusters were derived on the  $V$ -band mosaic image sub-frames of  $20'' \times 20''$  size using XGPHOT program implemented in IRAF (Tody 1993). The precise center coordinates of the clusters were determined from luminosity weighted profiles constructed in the central regions of the sub-frames of  $4'' \times 4''$  size. XGPHOT determines cluster's ellipticity and major axis position angle based on the second order moments of the luminosity distribution in the image. To determine the unbiased ellipticity and the position angle, we performed XGPHOT photometry in circular apertures from  $0.6''$  to the individual outer radii depending on the crowding degree of the neighborhood of each cluster. We used apertures of increasing size with a constant step of  $0.2''$  for all clusters. The plots of ellipticity and position angle versus radius were used to derive the final values of both parameters. We determined the ellipticity and the position angle by averaging these parameters over a "flat" range of radial parameter profiles.

For the final construction of the surface brightness profiles, we performed XGPHOT photometry in increasing elliptical apertures from  $0.1''$  out to  $8''$  radius, with a step of  $0.1''$  along the major axis. To overcome a small aperture size problem inherent to XGPHOT, the cluster sub-frames were sub-sampled by a factor of 10 using the IRAF *magnify* procedure.

The correct background estimate is essential for a reliable representation of the cluster surface brightness profiles, especially in their outer parts. The sky background was analyzed interactively for each cluster by searching for a representative region and varying its size. In some complex cases, additional corrections were applied, assuming a flat cluster surface brightness profile at large radii.

### 3.2. The analytical model profiles

The structural parameters of clusters were derived by fitting the King (1962) and the EFF (Elson et al. 1987) analytical models. The King model is defined by the central surface brightness,  $\mu_0$ , the core radius,  $r_c$ , and the tidal radius,  $r_t$ :

$$\mu(r) = \mu_0 \left[ \left( 1 + \frac{r^2}{r_c^2} \right)^{-1/2} - \left( 1 + \frac{r_t^2}{r_c^2} \right)^{-1/2} \right]^2. \quad (1)$$

The two following equations (Larsen 2006) were used to compute the cluster FWHM and half-light radii,  $r_h$ , from the King profile parameters:

$$\text{FWHM} = 2 \cdot r_c \left[ \left( \sqrt{1/2} + (1 - \sqrt{1/2})/\sqrt{1 + (r_t/r_c)^2} \right)^{-2} - 1 \right]^{1/2}, \quad (2)$$

$$r_h \approx 0.547 \cdot r_c (r_t/r_c)^{0.486}. \quad (3)$$

The EFF model is also defined by three parameters – the central surface brightness,  $\mu_0$ , the scale-length,  $r_e$ , and the power-law index,  $\gamma$ :

$$\mu(r) = \mu_0 \left( 1 + \frac{r^2}{r_e^2} \right)^{-\gamma/2}. \quad (4)$$

The three following equations (Larsen 2006) were used to compute FWHM and half-light radii,  $r_h$ , from the EFF profile parameters:

$$\text{FWHM} = 2 \cdot r_e \sqrt{2^{2/\gamma} - 1}, \quad (5)$$

$$r_h = r_e \sqrt{(1/2)^{2/(2-\gamma)} - 1}. \quad (6)$$

For the cases with  $\gamma \leq 2$  the total luminosity under the profile is infinite, and, therefore,  $r_h$  is undefined. In order to derive  $r_h$  in such extreme cases the surface brightness profiles must be truncated at some reasonably selected finite radii,  $r_m$ :

$$r_h = r_e \left[ \left[ 1/2 \left( (1 + r_m^2/r_e^2)^{(2-\gamma)/2} + 1 \right) \right]^{2/(2-\gamma)} - 1 \right]^{1/2}. \quad (7)$$

A discussion on the applicability and limitations of Equations (2), (3) and (5–7) for the determination of the cluster structural parameters is provided by Larsen (2006).

The analytical models (Equations 1 and 4) were fitted to the surface brightness profiles via  $\chi^2$  minimization. All parameters –  $\mu_0$ ,  $r_c$  and  $r_t$  for the King model, and  $\mu_0$ ,  $r_e$  and  $\gamma$  for the EFF model – were fitted simultaneously. The cluster profiles were fitted from the very center out to the radii from  $1.6''$  to  $4.6''$ , selected considering the cluster sizes and their neighborhood. For the clusters KWC 12, KWC 34 and KWC 44, which do not exhibit distinct centers, the inner fitting radius was set equal to  $1.8''$ ,  $1.2''$  and  $0.8''$ , respectively. The measured surface brightness

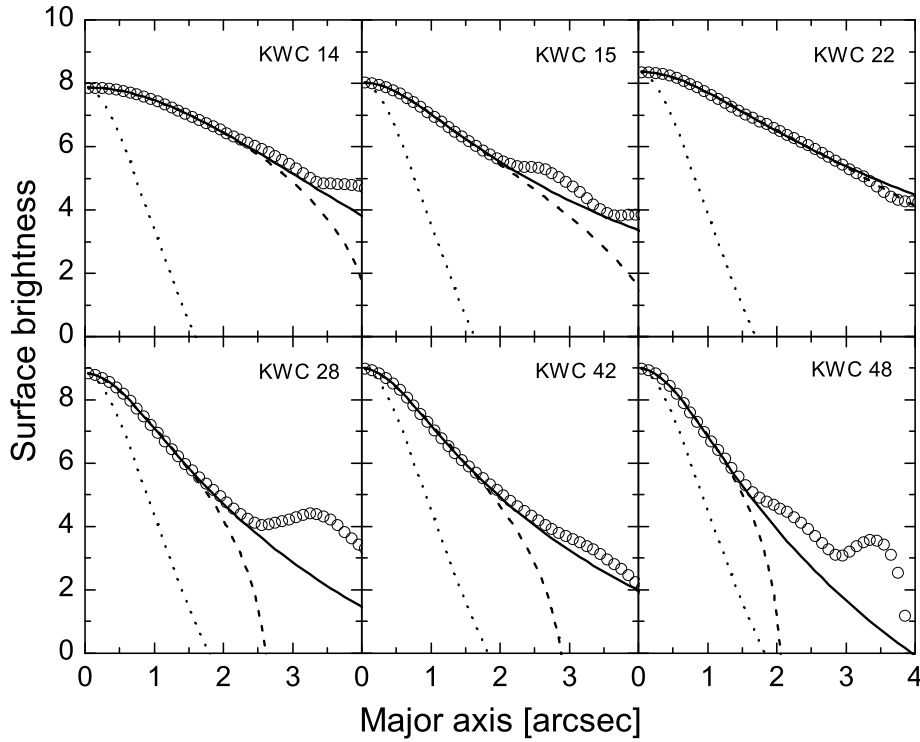


**Fig. 1.** The surface brightness profiles of the representative star clusters (in the instrumental magnitude scale) are shown by open circles. Solid and dashed lines mark the fitted EFF and King models, respectively; dotted lines are the averaged stellar profiles.

profiles and the fitted analytical models of six representative star clusters are shown in Figure 1. An averaged stellar profile is drawn in each panel.

### 3.3. Calibration grids of the cluster structural parameters

The cluster structural parameters derived from the 1-D surface brightness profiles are altered by the PSF effects. In order to eliminate these effects, the fitted cluster parameters were calibrated on the basis of simulated circular star clusters. We generated simulated cluster images with the surface brightness distribution of King (concentration factor  $r_t/r_c = 1.5 - 500$ ; a more conventional concentration parameter is usually defined as  $c = \log(r_t/r_c)$ ) and EFF ( $\gamma = 1 - 40$ ) models. The intrinsic FWHM of these simulated clusters varied in the range from  $0.1''$  to  $5.0''$ . FWHM and other structural parameters of the simulated clusters were inter-related by Equations (2) and (5). We convolved the simulated cluster images with the  $V$ -band mosaic PSF by means of the *imconvol* procedure in the BAO-LAB package producing large sets of the EFF and King model based simulated circular (ellipticity = 0.0) star clusters of different shapes and intrinsic sizes. PSF was constructed from well isolated stars in the field with the DAOPHOT (Stetson 1987) program set implemented in IRAF.

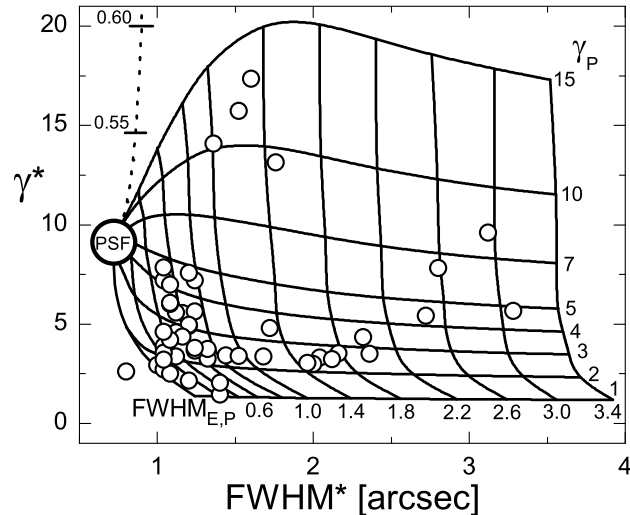


**Fig. 2.** The calibration grid of the cluster structural parameters fitted with the EFF model ( $\text{FWHM}^*$ ,  $\gamma^*$ ). Open circles mark the star clusters; the large circle is the PSF model; the dotted line is the locus of the simulated double stars with ticks indicating the separation between the components in FWHM units. The numbers on the right of the grid indicate the intrinsic power-law index,  $\gamma_P$ , and the numbers below the grid indicate the intrinsic  $\text{FWHM}_{E,P}$  (in arc-seconds) of the simulated clusters.

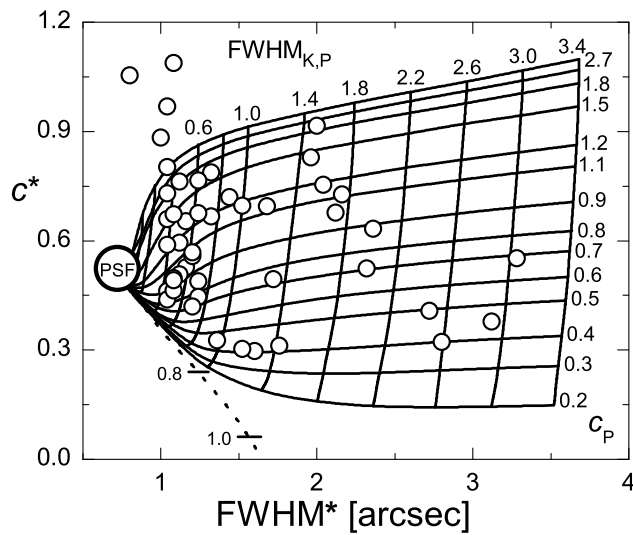


**Fig. 3.** The calibration grid of the cluster structural parameters fitted with the King model ( $\text{FWHM}^*$ ,  $c^*$ ). Open circles mark the star clusters; the large circle is the PSF model; the dotted line shows the locus of the simulated double stars with ticks indicating the separation between the components in FWHM units. The numbers on the right of the grid indicate the intrinsic concentration parameter,  $c_P$ , and the numbers on the top of the grid indicate the intrinsic  $\text{FWHM}_{K,P}$  (in arc-seconds) of the simulated clusters.

The same procedure as described in section 3.1 was applied to measure the simulated cluster images, however, all simulated clusters were measured in circular apertures. The clusters generated with the EFF profile were fitted with the EFF analytical model, and those generated with the King profile – with the King analytical model. The outer fitting radius for all the EFF model simulated clusters and for the King model simulated clusters of small intrinsic size ( $\text{FWHM} < 1.0''$ ) was equal to  $2.2''$ . For larger King model simulated clusters we applied a variable outer fitting radius of  $2.5 \times \text{FWHM}$ , in order to increase the accuracy of  $r_t$  determination.

To discriminate between star clusters and simply overlapping two stars (asterisms) we studied the 1-D profiles of simulated double stars. Double stars were constructed from two simulated stars (generated from PSF) of equal brightness placed at various separation distances. A procedure identical to that used for star clusters was applied to measure and fit the surface brightness profiles of the simulated double stars. The surface brightness profiles of double stars were fitted with the analytical models up to the outer radius of  $2.2''$ .

The calibration grids of the cluster structural parameters ( $\text{FWHM}^*$ ,  $\gamma^*$  for EFF;  $\text{FWHM}^*$  and  $c^*$  for King) fitted with analytical models versus the intrinsic ones ( $\text{FWHM}_{E,P}$ ,  $\gamma_P$  for EFF;  $\text{FWHM}_{K,P}$  and  $c_P$  for King) are shown in Figures 2 and 3. A position of PSF is indicated in the figures by a large open circle, marked ‘PSF’. The grid lines of both models converge to this point as expected for the objects of the smallest intrinsic size. Dotted lines in Figures 2 and 3 show the locus of the simulated double stars. Note a rapid increase of fitted  $\gamma^*$  and decrease of  $c^*$  with gradually increasing distance between the components of double stars. The star clusters and the simulated double stars fall in distinct regions of the grids, thus allowing the recognition of some asterisms.

The calibration grids shown in Figures 2 and 3 were employed to determine the intrinsic (free of alteration by PSF) structural parameters of clusters. A bilinear interpolation was used to derive the parameters  $\text{FWHM}_{E,P}$  and  $\gamma_P$  for the EFF models, and  $\text{FWHM}_{K,P}$  and  $c_P$  for the King models. The half-light radii of clusters,  $r_h$ , were computed by Eq. (6) ( $r_{h,E,P}$ ) and Eq. (3) ( $r_{h,K,P}$ ). For the extended clusters with  $\gamma_P < 3$  we used Eq. (7), instead of Eq. (6), and set the parameter  $r_m$  to be 4 times larger than the intrinsic FWHM of the cluster, providing a lower limit for the  $r_{h,E,P}$  estimate.

There are eight objects in our sample which fall outside the calibration grid in the King model parameter space shown in Figure 3 (four of them fall even outside the figure limits). These objects (KWC 02, KWC 09, KWC 10, KWC 16, KWC 19, KWC 24, KWE 33 and KWE 52) have much larger  $c^*$  values at a given  $\text{FWHM}^*$  than it could be derived from the simulated clusters. The same eight objects (Figure 2) have the EFF profile parameter  $\gamma_P < 2$  (luminosity integral diverges), suggesting very wide object wings. Note, that the largest object KWC 12 falls outside the parameter range shown in Figures 2 and 3, however, the accuracy of its structural parameters is high.

#### 4. RESULTS

In Figure 4 we compare the real intrinsic FWHM of star cluster derived from the calibration grids based on the EFF ( $\text{FWHM}_{E,P}$ ) and King ( $\text{FWHM}_{K,P}$ ) models. Both analytical models give well correlated FWHM – even the largest cluster in our sample, KWC 12, lies on the one-to-one correspondence line.

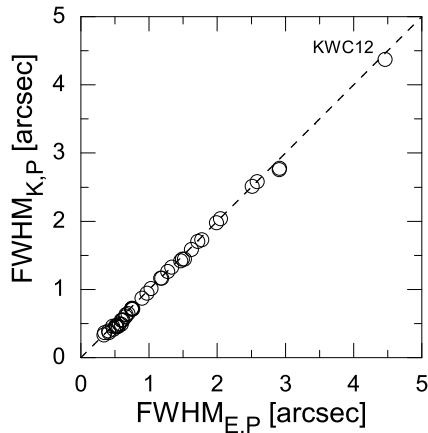


**Fig. 4.** The intrinsic FWHM of the clusters derived from the calibration grids based on the EFF ( $\text{FWHM}_{\text{E},\text{P}}$ ) and King ( $\text{FWHM}_{\text{K},\text{P}}$ ) models. The dashed line is the one-to-one relation.

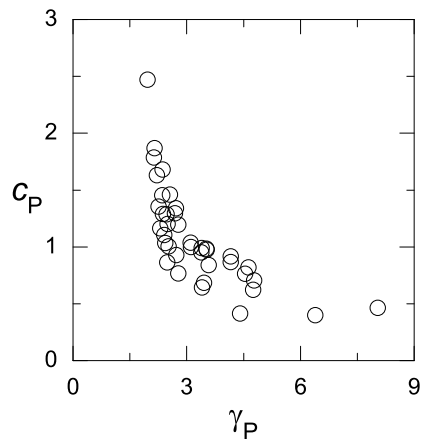


**Fig. 5.** The King model intrinsic concentration parameter,  $c_P$ , versus the EFF model intrinsic power-law index,  $\gamma_P$ , derived from the calibration grids.

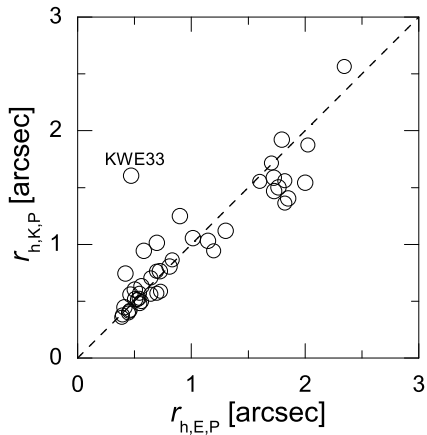


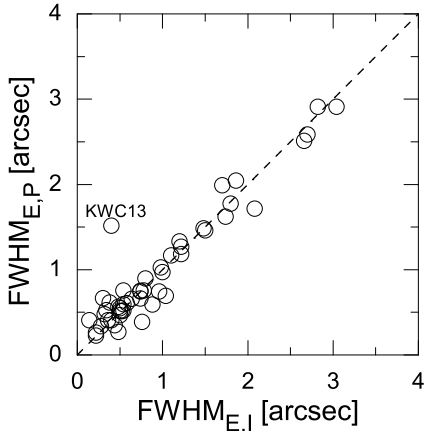
**Fig. 6.** Half-light radii of the star clusters computed from Eq. (3) ( $r_{\text{h},\text{K},\text{P}}$  – King) and Eqs. (6) or (7) ( $r_{\text{h},\text{E},\text{P}}$  – EFF). The dashed line in Figures 6–10 marks the one-to-one relation.

plotted. A tight correlation of the cluster intrinsic radius ( $r_h$ ) determined from the King model ( $r_{\text{h},\text{K},\text{P}}$ ) and the EFF model ( $r_{\text{h},\text{E},\text{P}}$ ) is shown in Figure 6. The deviating object, KWE33, is a young star cluster embedded in the HII region, which cannot be fitted properly with the King model.

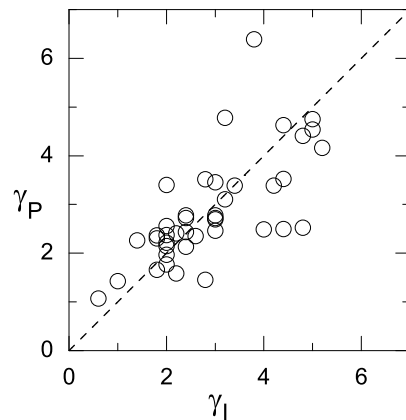
Comparisons of the cluster intrinsic parameters determined in this study (1-D profile) with those derived with ISHAPE from Paper II are shown in Figures 7–10. The largest cluster in our sample, KWC12, is omitted from these figures. Eight objects with unrealistically large  $\gamma$  derived with ISHAPE ( $\gamma_I > 7$ ) are not plotted. A tight correlation of the cluster intrinsic radius ( $r_h$ ) determined from the King model ( $r_{\text{h},\text{K},\text{P}}$ ) and the EFF model ( $r_{\text{h},\text{E},\text{P}}$ ) is shown in Figure 6. The deviating object, KWE33, is a young star cluster embedded in the HII region, which cannot be fitted properly with the King model.

Figure 5 also shows a rather tight correlation of the cluster EFF model power-law index,  $\gamma_P$ , with the King model concentration parameter,  $c_P$ , suggesting robustness of the derived structural parameters. Comparison of the cluster intrinsic  $r_h$  determined from the EFF (Eqs. (6)(or 7);  $r_{\text{h},\text{E},\text{P}}$ ) and King (Eq. 3;  $r_{\text{h},\text{K},\text{P}}$ ) model fits is shown in Figure 6. Note the larger (but still tolerable) scatter than in Figure 4. The deviating object, KWE33, is a young star cluster embedded in the HII region, which cannot be fitted properly with the King model.

Comparisons of the cluster intrinsic parameters determined in this study (1-D profile) with those derived with ISHAPE from Paper II are shown in Figures 7–10. The largest cluster in our sample, KWC12, is omitted from these figures. Eight objects with unrealistically large  $\gamma$  derived with ISHAPE ( $\gamma_I > 7$ ) are not plotted. A tight correlation of the cluster intrinsic radius ( $r_h$ ) determined from the King model ( $r_{\text{h},\text{K},\text{P}}$ ) and the EFF model ( $r_{\text{h},\text{E},\text{P}}$ ) is shown in Figure 6. The deviating object, KWE33, is a young star cluster embedded in the HII region, which cannot be fitted properly with the King model.



**Fig. 7.** Comparison of the cluster FWHM derived by fitting the EFF models with the 1-D profile ( $\text{FWHM}_{\text{E},\text{P}}$ ) and ISHAPE ( $\text{FWHM}_{\text{E},\text{I}}$ ) methods.



**Fig. 8.** Comparison of the cluster  $\gamma$ , derived by fitting the EFF models with the 1-D profile ( $\gamma_{\text{P}}$ ) and ISHAPE ( $\gamma_{\text{I}}$ ) methods.

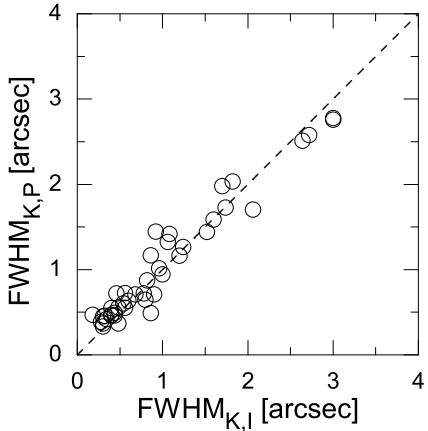


**Fig. 9.** Comparison of the cluster FWHM derived by fitting the King models with the 1-D profile ( $\text{FWHM}_{\text{K},\text{P}}$ ) and ISHAPE ( $\text{FWHM}_{\text{K},\text{I}}$ ) methods.

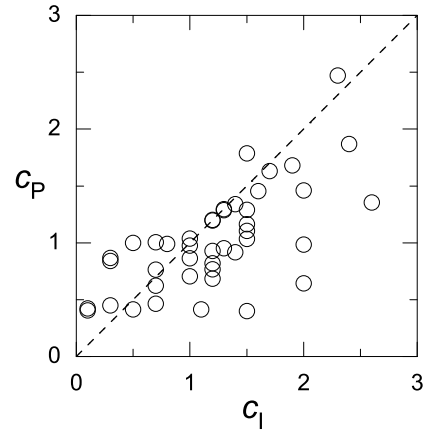


**Fig. 10.** Comparison of the cluster  $c$  derived by fitting the King models with the 1-D profile ( $c_{\text{P}}$ ) and ISHAPE ( $c_{\text{I}}$ ) methods. The formal accuracy of the concentration parameter,  $c_{\text{P}}$ , derived from 1-D profile fitting errors, typically is in the range of  $\pm(0.1\text{--}0.2)$ .

The only deviating object seen in Figure 7 is a very elongated background galaxy candidate, KWC13, the displacement of which may be due to circular simulated clusters used for constructing of the calibration grids. The cluster parameters,  $\gamma$  ( $\gamma_{\text{P}}, \gamma_{\text{I}}$ ) and  $c$  ( $c_{\text{P}}, c_{\text{I}}$ ), derived by both methods also correlate well (Figures 8 and 10). Note that all the objects deviating strongly from a one-to-one relation in Figures 8 and 10 cannot be fitted properly by one of the two methods (some clusters are too much resolved for ISHAPE, and some are too small for the

1-D profile method). The comparison suggests that the proposed method could effectively supplement ISHAPE, extending the workspace of star cluster parameter determination to the domain of semi-resolved objects. We find that our method could be applied for the analysis of star clusters whose intrinsic FWHM are larger than  $\sim 50\%$  of the FWHM of PSF.

We computed the final structural parameters of the clusters as weighted averages of the results from the 1-D profile (this study) and the ISHAPE (Paper II) method (Table 1). The parameter weights applied to different fitting methods depended on the cluster FWHM. For the smallest (unresolved) clusters ( $\text{FWHM} \leq 0.75''$ ) we applied higher weights to the ISHAPE results, and for the largest semi-resolved clusters ( $\text{FWHM} \geq 1.5''$ ) to the results of the 1-D surface brightness profile fits. For the intermediate size clusters (barely resolved) the results from both methods had comparable weights. The weights assigned to the fitting methods also varied, depending on the accuracy of the fitted parameters.

In Table 1 we provide FWHM averaged from the EFF and King model results, as well as individual values for respective analytical models ( $\text{FWHM}_E$ ,  $\gamma$  and  $\text{FWHM}_K$ ,  $c$ ) averaged from both methods (1-D profile and ISHAPE). We also give averaged  $r_h$  and individual ( $r_{h,E}$ ,  $r_{h,K}$ ) values for each analytical model, which were computed from the intrinsic ( $\text{FWHM}_E$  and  $\gamma$ ; Eq. (6 or 7), or  $\text{FWHM}_K$  and  $c$ ; Eq. (3)) parameters and averaged from both methods. Note that for nine clusters, which are not fitted by the King model reliably, only half-light radii,  $r_h$ , derived from the EFF model are provided.

In the  $r_h$  vs.  $M_V$  diagram (Figure 11; van den Bergh & Mackey 2004), star clusters from our sample occupy the region of fainter magnitudes than M 31 clusters studied by Barmby, Holland & Huchra (2002) and Barmby et al. (2007), and partly overlap with the parameter region of the Milky Way globular clusters (Harris 1996). The clusters in our sample are brighter than  $V \approx 19.5$ , therefore, a cut at  $M_V \approx -5$  is due to the selection effect. The clusters brighter than  $V \approx 17$  were saturated on Suprime-Cam images, therefore, they were also omitted from our sample. Note, however, that  $M_V$  does not translate directly into the cluster mass, because of a wide range of their ages. The clusters from the current study span a slightly wider half-light radius ( $r_h$ ) range than the clusters studied by Barmby et al. (2002, 2007), who selected only bright and concentrated “high probability” globular clusters.

**Table 1.** The structural parameters of the star clusters.

Cluster	$\text{FWHM}_E$	$\gamma$	$r_{h,E}$	$\text{FWHM}_K$	$c$	$r_{h,K}$	FWHM	$r_h$
KWC 01	0.54	5.2	0.36	0.30	1.40	0.41	0.42	0.38
KWC 02	0.24	1.9	0.48	0.24	–	–	0.24	0.48
KWC 03	0.58	4.2	0.43	0.56	0.80	0.43	0.57	0.43
KWC 04	0.69	3.1	0.73	0.70	0.90	0.58	0.69	0.66
KWC 05	0.50	4.4	0.36	0.32	1.20	0.35	0.41	0.36
KWC 06	1.30	>9	0.73	1.27	0.41	0.77	1.29	0.75
KWC 07	0.54	3.4	0.49	0.40	1.30	0.49	0.47	0.49
KWC 08	1.70	3.8	1.38	1.61	0.90	1.34	1.65	1.36
KWC 09	0.22	1.8	0.47	0.34	–	–	0.28	0.47
KWC 10	0.48	2.2	0.80	0.46	–	–	0.47	0.80
KWC 11	0.59	4.2	0.44	0.49	0.87	0.40	0.54	0.42
KWC 12	4.46	>9	2.52	4.37	0.30	2.57	4.42	2.55

**Table 1.** Continued

Cluster	FWHM <sub>E</sub>	$\gamma$	$r_{h,E}$	FWHM <sub>K</sub>	$c$	$r_{h,K}$	FWHM	$r_h$
KWC 13	1.52	2.3	2.38	1.20	—	—	1.36	2.38
KWC 14	2.64	5.2	1.76	2.60	0.60	1.73	2.62	1.74
KWC 15	1.20	2.4	1.78	1.20	1.30	1.47	1.20	1.62
KWC 16	0.41	1.1	1.42	1.58	—	—	0.41	1.42
KWC 17	0.40	2.6	0.63	0.30	1.55	0.48	0.35	0.55
KWC 18	0.50	2.4	0.74	0.44	1.50	0.66	0.47	0.70
KWC 19	0.76	2.8	1.02	0.66	1.40	0.89	0.71	0.96
KWC 20	1.46	>9	0.83	1.42	0.42	0.86	1.44	0.85
KWC 21	0.75	2.2	1.24	0.75	1.67	1.35	0.75	1.30
KWC 22	1.78	2.9	2.28	1.75	1.10	1.75	1.77	2.02
KWC 23	1.49	2.3	2.33	1.50	1.30	1.83	1.50	2.08
KWC 24	0.67	1.4	1.89	1.34	—	—	0.67	1.89
KWC 25	0.75	3.6	0.64	0.71	0.84	0.56	0.73	0.60
KWC 26	0.97	>9	0.55	0.94	0.46	0.58	0.95	0.56
KWC 27	0.34	2.8	0.46	0.18	2.00	0.47	0.26	0.46
KWC 28	0.64	3.2	0.64	0.54	1.00	0.49	0.59	0.57
KWC 29	0.85	2.2	1.41	0.84	1.40	1.14	0.84	1.27
KWC 30	2.51	4.4	1.82	2.55	0.60	1.69	2.53	1.76
KWC 31	0.77	4.8	0.53	0.69	0.72	0.50	0.73	0.51
KWC 32	2.05	2.8	2.70	2.00	1.00	1.82	2.02	2.26
KWC 33	0.50	3.0	0.56	0.42	1.20	0.46	0.46	0.51
KWC 34	2.91	8.0	1.71	2.80	0.50	1.76	2.86	1.73
KWC 35	0.30	2.1	0.53	0.30	—	—	0.30	0.53
KWC 36	1.20	>9	0.68	1.00	0.46	0.62	1.10	0.65
KWC 37	0.50	2.1	0.88	0.50	1.80	1.04	0.50	0.96
KWC 38	1.25	3.2	1.25	1.20	1.00	1.09	1.23	1.17
KWC 39	0.74	4.4	0.54	0.60	1.20	0.66	0.67	0.60
KWC 40	1.99	3.4	1.82	1.95	0.75	1.44	1.97	1.63
KWC 41	1.00	2.3	1.56	1.00	1.30	1.22	1.00	1.39
KWC 42	0.48	2.4	0.71	0.44	1.40	0.60	0.46	0.65
KWC 43	0.40	2.3	0.63	0.36	1.80	0.75	0.38	0.69
KWC 44	2.91	4.7	2.03	2.80	0.65	1.92	2.86	1.98
KWC 45	0.54	3.2	0.54	0.46	1.00	0.42	0.50	0.48
KWC 46	2.00	3.5	1.77	2.00	0.95	1.74	2.00	1.75
KWC 47	0.74	3.0	0.84	0.60	1.30	0.73	0.67	0.78
KWC 48	0.52	4.4	0.38	0.42	1.00	0.38	0.47	0.38
KWC 49	0.36	3.0	0.41	0.32	1.30	0.39	0.34	0.40
KWE 33	0.44	2.1	0.78	0.48	—	—	0.46	0.78
KWE 52	0.14	2.2	0.23	0.10	—	—	0.12	0.23

**Note:** FWHM – the averaged final FWHM; FWHM<sub>E</sub> and FWHM<sub>K</sub> – FWHM derived from the EFF and King models, respectively (in arc-seconds);  $\gamma$  – the EFF model power-law index;  $c$  – the King model concentration parameter,  $c = \log(r_t/r_c)$ ;  $r_h$  – the averaged final half-light radius;  $r_{h,E}$  and  $r_{h,K}$  – the half-light radii derived from the EFF and King models, respectively (in arc-seconds). The final FWHM and  $r_h$  (presented in the last two columns) are derived by averaging FWHM<sub>E</sub> and FWHM<sub>K</sub>;  $r_{h,E}$  and  $r_{h,K}$ , respectively.

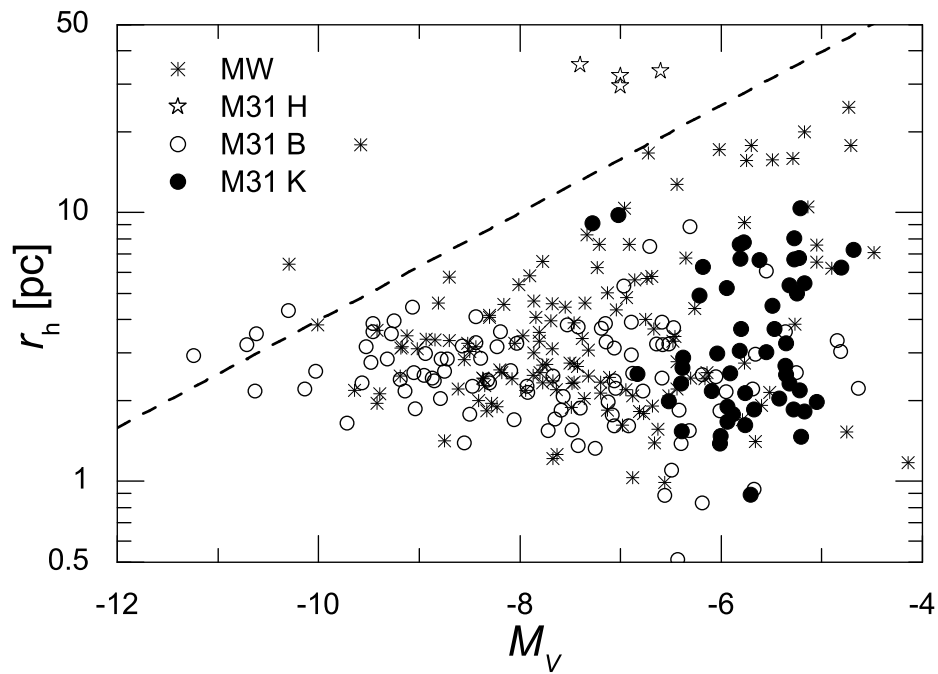


**Fig. 11.** Plot of the cluster  $r_h$  versus  $M_V$ . Filled circles mark the M 31 clusters from our sample; open circles – from Barmby et al. (2002, 2007); open stars – the extended M 31 clusters from Mackey et al. (2006). The Milky Way globular clusters (Harris 1996; catalog revision: February 2003) are shown by asterisks. The dashed line represents the equation  $\log(r_h) = 0.2 M_V + 2.6$  (van den Bergh & Mackey 2004).

## 5. SUMMARY

We apply the 1-D surface brightness profile fitting method to determine structural parameters of star clusters by fitting the King and the EFF models and demonstrate its performance on 51 cluster candidates from the survey of compact star clusters in the M 31 disk (Paper I). The structural parameters of clusters are derived from the  $V$ -band images using the calibration grids based on simulated star clusters.

A set of simulated clusters with predefined structural parameters was generated and convolved with the  $V$ -band PSF. The surface brightness profiles of the simulated clusters were derived from the aperture photometry data, and their structural parameters were determined by fitting the analytical EFF and King models in the same manner as for the real star clusters. The structural parameter calibration grids were constructed on the basis of the simulated cluster data.

We find that the 1-D surface brightness profile fitting method works well for the majority of clusters in our sample. The derived intrinsic FWHM and half-light radii,  $r_h$ , are virtually independent on the analytical models employed. The structural parameters determined in this study (1-D profile fit) are in good agreement with those derived for the same star clusters by ISHAPE (Paper II). Therefore we conclude that the 1-D profile fitting method is a robust tool for the determination of structural parameters of star clusters, and may be effectively applied for the

analysis of clusters whose intrinsic FWHM are larger than  $\sim 50\%$  of the FWHM of PSF.

**ACKNOWLEDGMENTS.** We are thankful to our referee S. Larsen for his constructive suggestions. This work was financially supported in part by a Grant of the Lithuanian State Science and Studies Foundation. The research has made use of SAOImage DS9, developed by the Smithsonian Astrophysical Observatory.

## REFERENCES

- Barmby P., Holland S., Huchra J. 2002, AJ, 123, 1937  
 Barmby P., McLaughlin D. E., Harris W. E., Harris G. L. H., Forbes D. A. 2007,  
     AJ, 133, 2764  
 Elson R. A. W., Fall S. M., Freeman K. C. 1987, ApJ, 323, 54  
 Harris W. E. 1996, AJ, 112, 1487  
 Hill A., Zaritsky D. 2006, AJ, 131, 414  
 King I. 1962, AJ, 67, 471  
 Kodaira K., Vansevičius V., Bridžius A., Komiyama Y., Miyazaki S., Stonkutė R.,  
     Šablevičiūtė I., Narbutis D. 2004, PASJ, 56, 1025 (Paper I)  
 Larsen S. S. 1999, A&AS, 139, 393  
 Larsen S. S. 2006, *An ISHAPe User's Guide* (ver. Oct. 23, 2006; available at  
     <http://www.astro.uu.nl/~larsen/baolab/>), p. 14  
 Mackey A. D., Huxor A., Ferguson A. M. N. et al. 2006, ApJ, 653, L105  
 Miyazaki S., Komiyama Y., Sekiguchi M. et al. 2002, PASJ, 54, 833  
 Narbutis D., Vansevičius V., Kodaira K., Šablevičiūtė I., Stonkutė R., Bridžius A.  
     2006, Baltic Astronomy, 15, 461  
 Šablevičiūtė I., Vansevičius V., Kodaira K., Narbutis D., Stonkutė R., Bridžius A.  
     2006, Baltic Astronomy, 15, 547 (Paper II)  
 Stanek K. Z., Garnavich P. M. 1998, ApJ, 503, L131  
 Stetson P. B. 1987, PASP, 99, 191  
 Tody D. 1993, in *Astronomical Data Analysis Software and Systems II*, eds. R. J. Hanisch,  
     R. J. B. Brissenden, J. Barnes, ASP Conf. Ser. 52, ASP, San Francisco, 173  
 van den Bergh S., Mackey A. D. 2004, MNRAS, 354, 713